Optimizing Process Parameters of As-Homogenized Mg-Gd-Y-Zn-Zr Alloy in Isothermal Uniaxial Compression on the Basis of Processing Maps via Prasad Criterion and Murty Criterion

Qiang Chen, Li Hu ⓘ, Mingao Li, Yong Chen, Laixin Shi, Tao Zhou, and Mingbo Yang

Isothermal compression experiments of as-homogenized Mg-8.5Gd-4.5Y-0.8Zn-0.4Zr alloy are conducted at temperature range of 673-773 K (400-500 °C) and strain rate range of 0.001-1 s^{-1} in order to identify the optimized processing parameters. Results show that flow stress decreases with the decreasing strain rate at a given temperature and increases with the decreasing temperature at a specific strain rate. Based on the obtained true stress-strain curves, processing maps based on the Prasad criterion and the Murty criterion are separately constructed. Obviously, distributions of power dissipation and the instability regime in the case of the Prasad criterion are different from the corresponding ones in the case of the Murty criterion during hot deformation. Microstructure observations on deformed samples confirm that kink band and dynamic recrystallization, rather than microcrack and flow localization, occur at 698 K and 0.01 s^{-1}. This issue verifies the accuracy of instability regions determined on the base of the Murty criterion. Consequently, the processing window determined on the base of the Murty criterion is more reliable than that identified on the base of the Prasad criterion. The optimized processing parameters are finally ascertained to be 698-748 K, 0.001-0.01 s^{-1}, and 748-773 K, 0.01-0.1 s^{-1}.

1. Introduction

As a typical representative of magnesium-rare earth (Mg-RE) alloy, Mg-Gd-Y-Zn-Zr alloy has been termed as a potential candidate for substituting aluminum alloys and steels in aircraft and space apparatus construction due to its low density, remarkable strength, high-temperature stability, and superior creep resistance (Ref 1-3). For example, Homma et al. (Ref 4) successfully fabricated a high-strength Mg-1.8Gd-1.8Y-0.7Zn-0.2Zr alloy by hot extrusion and subsequent aging treatment. The fabricated material possesses an ultimate strength of 542 MPa, 0.2% proof stress of 473 MPa, and elongation to failure of 8.0%. Xu et al. (Ref 5) manufactured a high-strength Mg-8.2Gd-3.8Y-1.0Zn-0.4Zr alloy via hot rolling followed by aging process. The obtained sheet exhibits outstanding tensile properties with ultimate strength of 517 MPa, 0.2% proof stress of 426 MPa, and elongation to failure of 4.5%.

However, owing to its intrinsic characteristic of hexagonal close-packed (HCP) structure, Mg-Gd-Y-Zn-Zr alloy also possesses a perceived weakness of poor formability at ambient temperature (Ref 6, 7). Therefore, cold working cannot be served as a proper approach to fabricate products of Mg-Gd-Y-Zn-Zr alloy. By comparison, hot working has been considered to be a desired method to manufacture Mg-Gd-Y-Zn-Zr alloy products as the workability of Mg-Gd-Y-Zn-Zr alloy could be obviously enhanced at elevated temperature. Furthermore, it has been generally accepted that the quality of hot working is highly sensitive to the extremely complex nonlinear-relationship between processing parameters and initial microstructure characteristics of the studied alloy (Ref 8). Many pioneer works have confirmed that the processing map based on the dynamic materials model (DMM) is a powerful tool in optimizing hot working parameters and controlling the microstructure of Mg alloys (Ref 9-11). Therefore, to achieve the high-dimensional accuracy and satisfactory mechanical properties of fabricated components, it is imperative to investigate the hot deformation behavior, construct the corresponding processing map and finally identify the reasonable processing window of Mg-Gd-Y-Zn-Zr alloy.

Nowadays, there mainly exist two mainstream approaches with regard to constructing processing map of metallurgical materials during hot deformation. Namely, processing map can be constructed by using either the Prasad criterion or the Murty criterion (Ref 12). Both of them obey the continuum mechanics and irreversible thermodynamics theories. The input power P (per unit volume) of the hot working piece can be additively decomposed into the dissipative quantity (G) and the dissipative co-quantity (J) by the following equation (Ref 13, 14):

Qiang Chen, Southwest Technology and Engineering Research Institute, Chongqing 400039, China; **Li Hu, Mingao Li, Laixin Shi, Tao Zhou,** and **Mingbo Yang**, College of Material Science and Engineering, Chongqing University of Technology, Chongqing 400054, China; **Yong Chen**, Key Laboratory of Advanced Manufacturing Technology for Automobile Parts, Ministry of Education, Chongqing University of Technology, Chongqing 400054, China. Contact e-mail: huli@cqut.edu.cn.

$$P = \sigma\dot{\varepsilon} = G + J = \int_0^{\dot{\varepsilon}} \sigma\, \mathrm{d}\dot{\varepsilon} + \int_0^{\sigma} \dot{\varepsilon}\, \mathrm{d}\sigma \qquad \text{(Eq 1)}$$

where G reflects the energy of the material consumed by plastic work, and it would mainly result in the temperature rise of hot working piece. J represents the energy dissipated by microstructure evolution during hot deformation process.

Under certain conditions with constant strain (ε) and temperature (T), the change of J with respect to G characterizes the well-known strain rate sensitivity parameter m:

$$m = \frac{\mathrm{d}J}{\mathrm{d}G} = \left[\frac{\partial(\ln\sigma)}{\partial(\ln\dot{\varepsilon})}\right]_{\varepsilon,T} \qquad \text{(Eq 2)}$$

where m reaches its maximum value of 1 in the case of an ideal linear dissipation process. This aspect indicates that J can also possess its maximum value of J_{max} when $m = 1$. Therefore, the specific form of J_{max} can be depicted as $J_{max} = \sigma\dot{\varepsilon}/2$.

The definition of efficiency of power dissipation η is introduced to evaluate the dissipative characteristics of the material during hot working process by the following equation:

$$\eta = \frac{J}{J_{max}} = \frac{(P-G)}{J_{max}} = 2 - \frac{G}{J_{max}} \qquad \text{(Eq 3)}$$

It is clear that the calculation of η is highly related to the corresponding value of $G = \int \sigma\, \mathrm{d}\dot{\varepsilon}$. The methodology to tackle the integral operation is the fundamental difference between the Prasad criterion and the Murty criterion. In fact, Prasad et al. (Ref 13) supposed that m is independent of $\dot{\varepsilon}$ at specific temperature, and the flow stress curve follows the power law by the following equation:

$$\sigma = K\dot{\varepsilon}^m \qquad \text{(Eq 4)}$$

where K and m are material constants here. Using Eq 4, the dissipative quantity G can be further expressed as:

$$G = \int_0^{\dot{\varepsilon}} \sigma\, \mathrm{d}\dot{\varepsilon} = \int_0^{\dot{\varepsilon}} K\dot{\varepsilon}^m\, \mathrm{d}\dot{\varepsilon} = \frac{K\dot{\varepsilon}^{m+1}}{m+1} = \frac{\sigma\dot{\varepsilon}}{m+1} \qquad \text{(Eq 5)}$$

Using Eq 3-5, η can be written in terms of m as:

$$\eta = \frac{2m}{m+1} \qquad \text{(Eq 6)}$$

Based on the continuum principles of large plastic flow, Prasad et al. (Ref 15) proposed the instability criterion by defining the dimensionless parameter (ξ) as:

$$\xi = \frac{\partial \ln[m/(m+1)]}{\partial \ln\dot{\varepsilon}} + m \qquad \text{(Eq 7)}$$

where the instability domain is distinguished as zone with $\xi < 0$, while the remaining part is termed as the safe domain.

Unlike to the Prasad criterion, Murty et al. (Ref 14, 16) considered that as for a complicated alloy system, the relationship between flow stress and strain rate does not follow the power law yet. Namely, m varies with $\dot{\varepsilon}$ and T. Based on the work of Murty, a new criterion, which is applicable to any kinds of σ versus $\dot{\varepsilon}$ curves, is proposed. The calculation of G in Eq 1 can be expressed as:

$$G = \int_0^{\dot{\varepsilon}} \sigma\, \mathrm{d}\dot{\varepsilon} = \int_0^{\dot{\varepsilon}_{min}} \sigma\, \mathrm{d}\dot{\varepsilon} + \int_{\dot{\varepsilon}_{min}}^{\dot{\varepsilon}} \sigma\, \mathrm{d}\dot{\varepsilon} = \left[\frac{\sigma\dot{\varepsilon}}{m+1}\right]_{\dot{\varepsilon}=\dot{\varepsilon}_{min}} + \int_{\dot{\varepsilon}_{min}}^{\dot{\varepsilon}} \sigma\, \mathrm{d}\dot{\varepsilon} \qquad \text{(Eq 8)}$$

where $\dot{\varepsilon}_{min}$ refers to the minimal value of strain rate during hot working process. In the absence of experimental data about flow stress in the case of $0 < \dot{\varepsilon} < \dot{\varepsilon}_{min}$, it is assumed that σ versus $\dot{\varepsilon}$ curve obeys the power law as depicted in Eq 4. With this assumption, the integral operation of $\int_0^{\dot{\varepsilon}_{min}} \sigma\, \mathrm{d}\dot{\varepsilon}$ is replaced by $\left[\frac{\sigma\dot{\varepsilon}}{m+1}\right]_{\dot{\varepsilon}=\dot{\varepsilon}_{min}}$.

By substituting Eq 8 into Eq 3, a non-dimensional parameter η can be obtained as:

$$\eta = 2\left[1 - \left(\left[\frac{\sigma\dot{\varepsilon}}{m+1}\right]_{\dot{\varepsilon}=\dot{\varepsilon}_{min}} + \int_{\dot{\varepsilon}_{min}}^{\dot{\varepsilon}} \sigma\, \mathrm{d}\dot{\varepsilon}\right) \Big/ \sigma\dot{\varepsilon}\right] \qquad \text{(Eq 9)}$$

Moreover, according to the extremum principle of irreversible thermodynamics as applied to large plastic flow, Murty et al. (Ref 16) proposed their criterion considering the appearance of flow instability as:

$$2m < \eta < 0 \qquad \text{(Eq 10)}$$

Using Eq 6 and 7, a complete description of processing map based on the Prasad criterion has been realized, while the same would be done by combining Eq 9 and 10 for the construction of processing map based on the Murty criterion. As expected, processing maps based on the Prasad criterion and the Murty criterion would exhibit some differences, which may influence the determination of optimized hot working parameters. However, literature search demonstrates that as for Mg alloys, there exist few comparative studies about the capability of process optimization on the base of the Prasad criterion and the Murty criterion.

The present study aims to address this issue. Based on the isothermal compression experiments conducted among the chosen ranges of temperature and strain rate, the hot deformation behavior of selected Mg-Gd-Y-Zn-Zr alloy is obtained and analyzed. Afterward, processing maps based on the Prasad criterion and the Murty criterion are separately constructed. Subsequently, in-depth investigations on the differences of these two processing maps at various strain values are conducted. Finally, with the assistance of microstructure characterization of deformed samples, the optimized processing parameters are determined.

2. Material and Methods

The studied material in the present study is the as-received Mg-8.5Gd-4.5Y-0.8Zn-0.4Zr (wt.%) alloy in the form of an extruded plate. To obtain a homogenized microstructure with as few precipitates as possible, solid solution treatment at 773 K (500 °C, Kelvin temperature = Centigrade temperature + 273)/ 12 h was conducted on these as-received plates. Afterwards, cylinder samples were cut from these solution-treated plates along the extrusion direction (ED) by means of electro-discharge machining (EDM). The corresponding dimensions were determined to be 8 mm in diameter and 12 mm in height.

According to the applied deformation conditions reported in the work of Zhou et al. (Ref 3), uniaxial compression experiments in the present study were then conducted on a Gleeble-1500d thermo mechanical simulator at the temperature range of 673-773 K with an interval of 25 K and the strain rate range of 0.001-1 s^{-1} with an interval of one order of magnitude. To guarantee the uniformity of temperature within these heated samples, a small heating rate of 2 K/s and a long holding time of 300 s were applied in the present study. Before compression, an appropriate amount of graphite was coated on the top and bottom surfaces of samples to ensure a good lubrication state. All samples were compressed to the true strain of 0.70, subsequently followed by quenching into the cold water in order to keep the deformed microstructure. Figure 1 displays the macroscopic pictures of all compressed samples after isothermal compression experiments. It is obvious that these compressed samples possess drum-shaped characteristics, especially under the condition of the high strain rate. This issue is closely related to the friction effect on the upper and lower surfaces during uniaxial compression and indicates the inhomogeneous distribution of plastic deformation within these compressed samples. Subsequently, these undeformed and deformed samples were halved along the loading axis by

EDM, and then mechanically polished by SiC paper and chemically etched in the chosen solution containing 1g oxalate, 1ml nitric acid and 98 mL H$_2$O. Finally, microstructure observations on the central regions of these samples were carried out by using a Leica DMI5000M metallographic microscope and a FEI NOVA 400 Zeiss Sigma field emission scanning electron microscope (SEM) equipped energy dispersive spectroscopy (EDS).

3. Results and Discussion

3.1 Microstructure of Solution-Treated Sample Before Hot Compression

Figure 2 shows the microstructure characteristics of as-homogenized Mg-8.5Gd-4.5Y-0.8Zn-0.4Zr alloy and the corresponding analysis of elemental constituents. It is clear in Fig. 2(a) that the solution-treated material possesses an equiaxed microstructure with an average grain size of about 30.9 μm. A more detailed characterization of microstructure is displayed in Fig. 2(b). Obviously, there exist some chunky phases marked by points 2 and 3 and cubic phases marked by
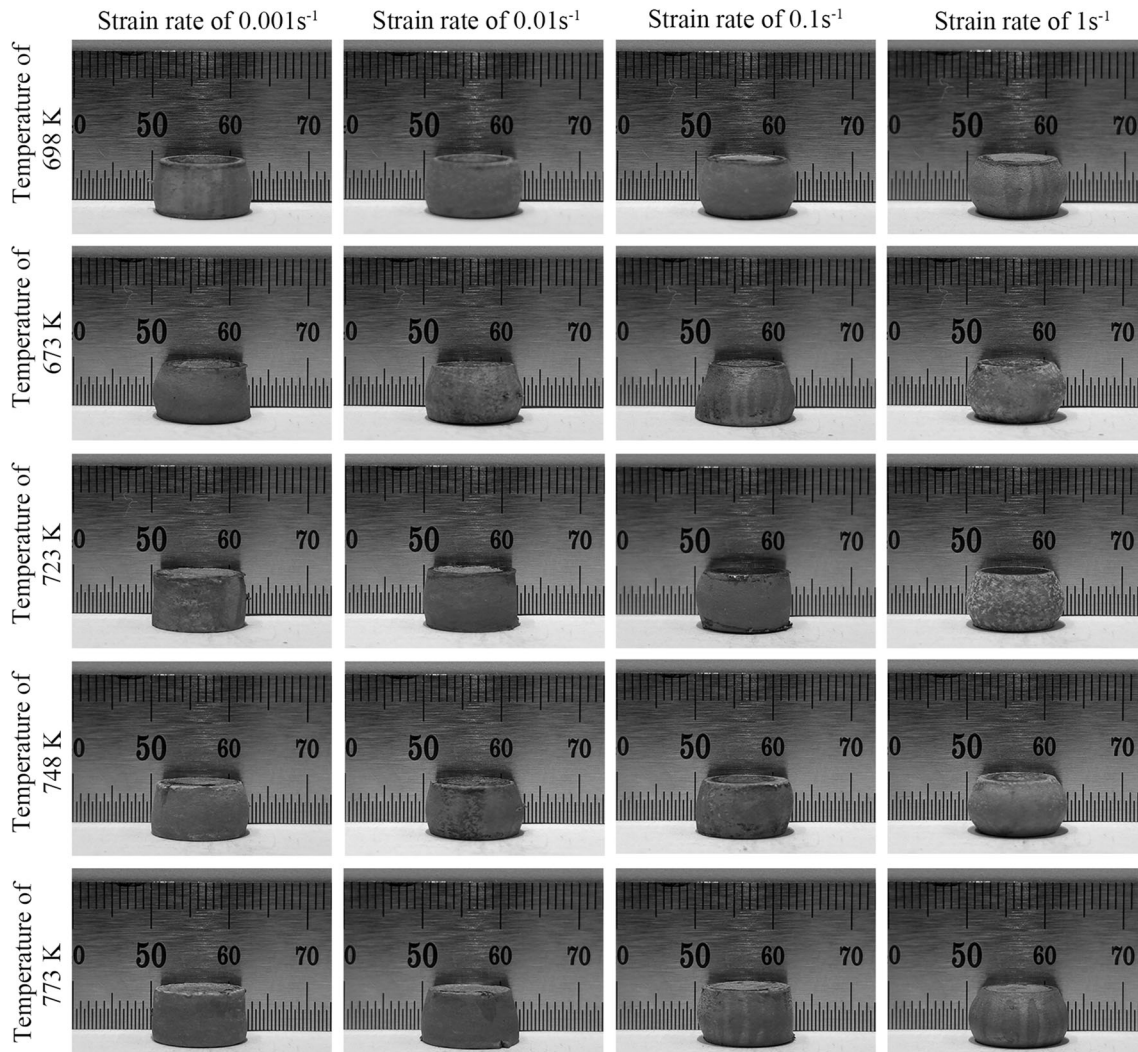

Fig. 1. Photographs showing the shape characteristics of these compressed samples at the true strain of 0.70
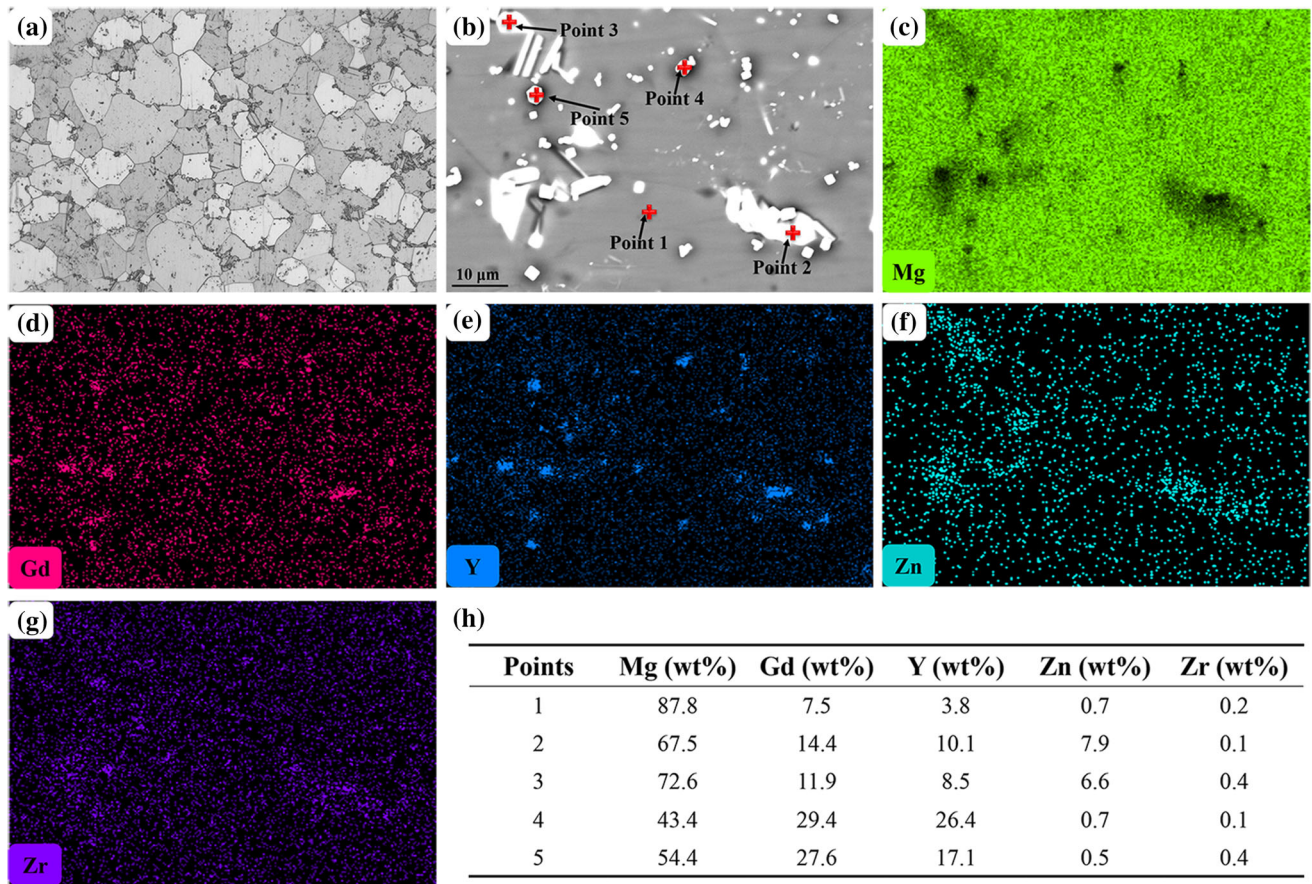
Fig. 2. Microstructure characteristics of solution-treated sample: (a) Optical observation of microstructure; (b) SEM observation of microstructure; (c-g) EDS maps of (b); (h) Point analysis taken from (b)

Points	Mg (wt%)	Gd (wt%)	Y (wt%)	Zn (wt%)	Zr (wt%)
1	87.8	7.5	3.8	0.7	0.2
2	67.5	14.4	10.1	7.9	0.1
3	72.6	11.9	8.5	6.6	0.4
4	43.4	29.4	26.4	0.7	0.1
5	54.4	27.6	17.1	0.5	0.4

points 4 and 5 within the matrix of the solution-treated sample highlighted by point 1. The corresponding EDS maps of constituent elements are displayed in Fig. 2(c), (d), (e), (f), and (g), showing a heterogeneous distribution of constituent elements. Furthermore, point analysis on these selected points are shown in Fig. 2(h). Points 2 and 3 are identified with a larger amount of Zn by comparison with other points, therefore these chunky phases are supposed to be 14H type of long period stacking ordered (LPSO) phase (Ref 3, 17). Moreover, points 4 and 5 possess a large amount of Gd and Y and a small amount of Zn and Zr. This observation confirms that these cubic phases within matrix belong to the RE-rich phase (Ref 18).

3.2 Flow Stress Behavior

The true stress-strain curves of as-homogenized Mg-8.5Gd-4.5Y-0.8Zn-0.4Zr alloy under various deformation conditions are presented in Fig. 3. It is obvious that the flow stress behavior of this material highly depends on temperature and strain rate. Namely, flow stress maintains a decreasing tendency with decreasing strain rate at a specific temperature and possess an increasing tendency with decreasing temperature at a given strain rate. Moreover, at the early stage of plastic deformation, flow stresses in all curves increase rapidly with increasing plastic strain. This issue is known as work hardening, which is mainly resulted from the multiplication of dislocation within Mg alloys during hot deformation (Ref 19). Soon after the arrival of peak stress (σ_p), all curves exhibit obvious decline

with increasing plastic strain. These characteristics of true stress-strain curves demonstrate the occurrence of dynamic flow softening, which is attributed to the restoration mechanism of dynamic recrystallization (DRX) for Mg alloys during hot deformation (Ref 20). Interestingly, under the deformation condition of temperature no more than 723 K and strain rate of 0.1 s^{-1}, stress oscillation can be obviously observed in the obtained true stress-strain curves. This phenomenon has also been reported by Xue et al. (Ref 10) and Zhou et al. (Ref 21). They confirmed that the occurrence of stress oscillation is closely related to the DRX behavior during hot deformation.

3.3 Analysis of Processing Maps

In the present study, MATLAB software is applied to operate the numerical calculation during constructing processing maps. The difficult point of processing map based on the Prasad criterion is the determination of the strain rate sensitivity parameter m and the dimensionless parameter ξ, as shown in Eq 6 and 7, respectively. This issue can be conveniently handled by using the gradient function of "Gradient" in MATLAB code. Furthermore, the key point of processing map based on the Murty criterion is the integral operation of the dissipative quantity G, as shown in Eq 8. This problem can be effectively settled by using the cumulative trapezoidal integral function of "Cumtrapz" in MATLAB code. The specific illustrations of function "Gradient" and function "Cumtrapz" are well documented in (Ref 22).
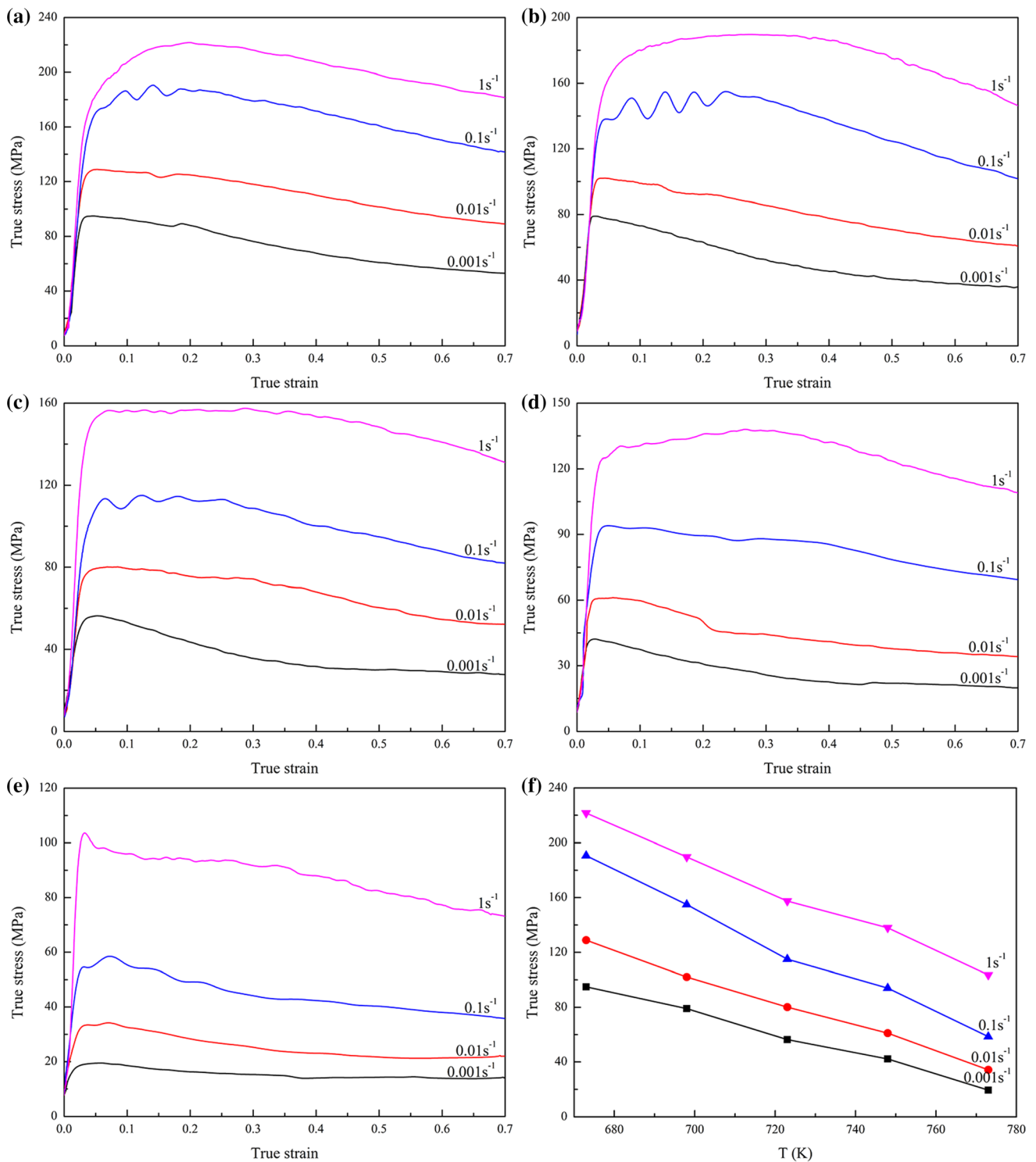
Fig. 3. True stress-strain curves of as-homogenized Mg-8.5Gd-4.5Y-0.8Zn-0.4Zr alloy under different temperatures: (a) 673K; (b) 698K; (c) 723K; (d) 748K; (e) 773K and (f) Relationship between peak stress and temperature

Figure 4 displays the 3D space distribution of power dissipation and the corresponding 2D planar contour on the base of the Prasad criterion and the Murty criterion. Moreover, the difference about power dissipation is also calculated and depicted here. Through comparing Fig. 4(a1), (b1), (c1), (d1), (e1), and (f1) and Fig. 4(a2), (b2), (c2), (d2), (e2), and (f2), it is clear that although the general distribution of power dissipation on the base of the Prasad criterion is similar to the correspond-

ing one on the base of the Murty criterion, there certainly exist some differences about the distribution of power dissipation in the processing region as plastic strain proceeds. Figure 4(a3), (b3), (c3), (d3), (e3), and (f3) provide overwhelming evidence for this issue. Obviously, three distinctive domains exist, namely the region with lower temperature and in-between strain rate (about 673-700 K, 0.1-0.01 s^{-1}), the region with higher temperature and lower strain rate (about 720-773 K, 0.01-
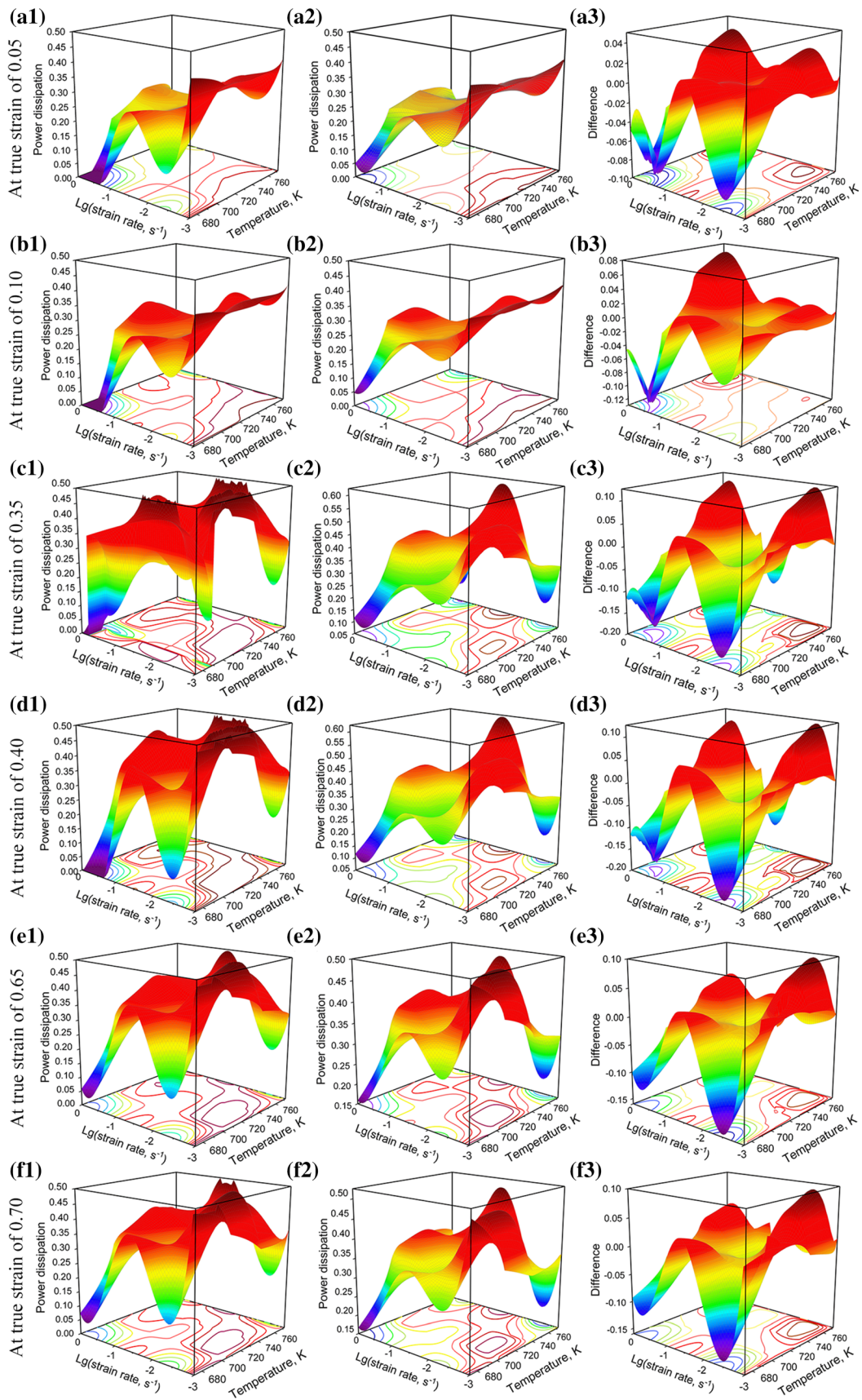
Fig. 4. Evaluation of the distribution of power dissipation associated with temperature and logarithmic strain rate under different true strains: (a1)-(f1) Based on the Prasad criterion; (a2)-(f2) Based on the Prasad criterion; (c3)-(f3) The corresponding differences

0.001 s^{-1}) and the region with higher temperature and higher strain rate (about 720-773 K, 0.1-1 s^{-1}).

Based on the identification rules of instability domain, as depicted in Eq 7 and 10, Fig. 5 demonstrates the instability regions based on the Prasad criterion and the corresponding ones based on the Murty criterion as well as the differences between them. It has been generally accepted that the instability domain indicates the occurrence of wedge cracking during hot deformation of metallic materials, and it should be excluded from the chosen deformation condition, which corresponds to good workability (Ref 23, 24). Fig. 5(a1), (b1), (c1), (d1), (e1), and (f1) illustrate that in the case of the Prasad criterion there mainly exist two instability regions, which are located in the area of lower temperature and lower strain rate (about 673-700 K, 0.01-0.001 s^{-1}) and the area of lower temperature and lower

higher strain rate (about 673-700 K, 0.1-1 s^{-1}). In addition, the scope of these instability domains on the basis of the Murty criterion, as shown in Fig. 5(a2), (b2), (c2), (d2), (e2), and (f2), is reduced by comparison with the corresponding ones on the base of the Prasad criterion. This observation can be further verified by investigating the differences between these calculated instability domains, as shown in Fig. 5(a3), (b3), (c3), (d3), (e3), and (f3).

Figure 6 depicts the processing maps of as-homogenized Mg-8.5Gd-4.5Y-0.8Zn-0.4Zr alloy in the case of the true strain of 0.70. The processing map is constructed via the superposition of the 2D planar contour of power dissipation map and instability map. It is obvious that no matter the processing map based on the Prasad criterion or the Murty criterion possesses specific instability regions overlapped on the low power
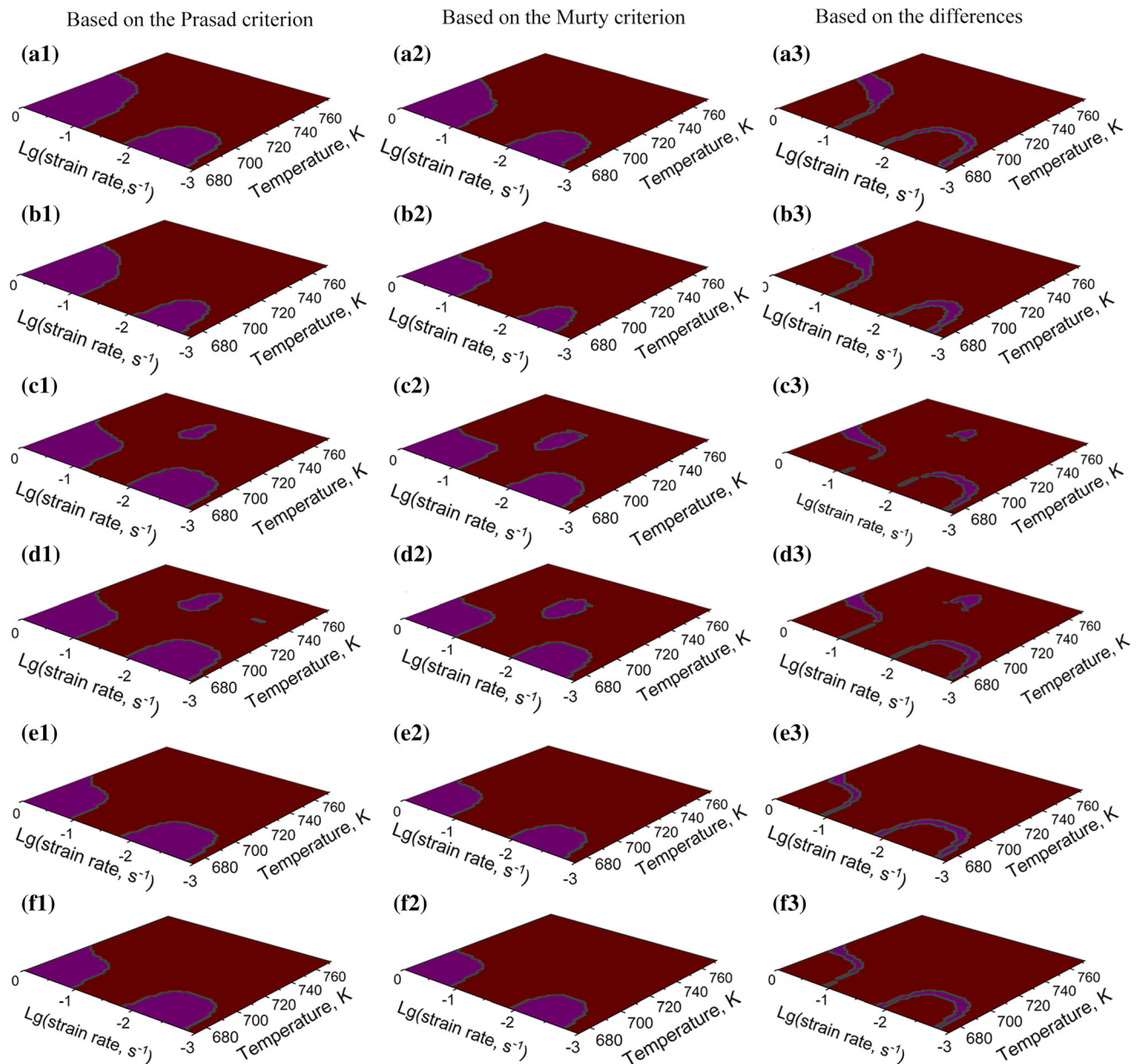

Fig. 5. Evaluation of instability regimes in temperature vs. logarithmic strain rate coordinate with the proceeding of plastic strain: (a1)-(a3) At true strain of 0.05; (b1)-(b3) At true strain of 0.10; (c1)-(c3) At true strain of 0.35; (d1)-(d3) At true strain of 0.40; (e1)-(e3) At true strain of 0.65; (f1)-(f3) At true strain of 0.70
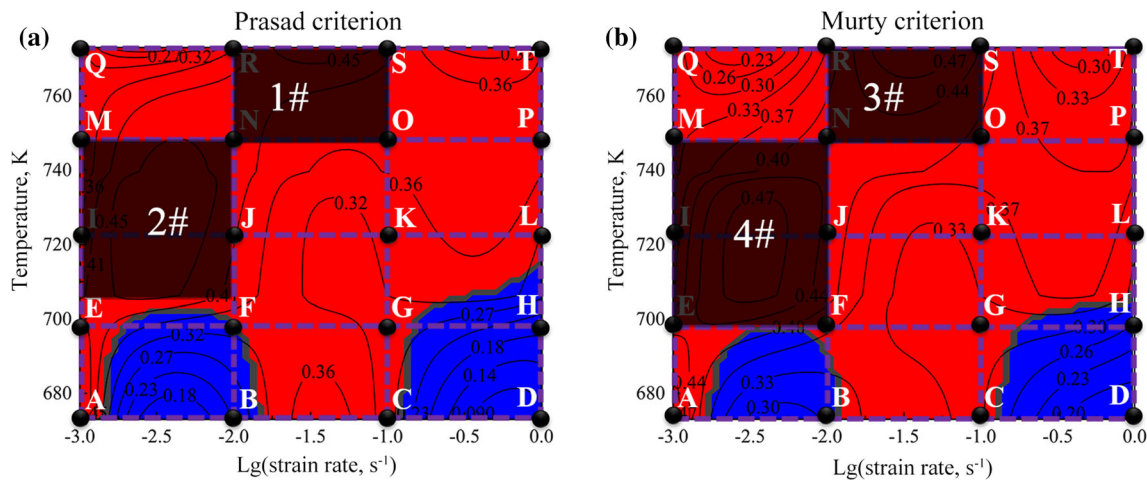
Fig. 6. Evaluation of processing maps in the case of the true strain of 0.70: (a) Based on the Prasad criterion; (b) Based on the Murty criterion (Horizontal and vertical dotted lines with purple color represent the applied deformation temperatures and strain rates, respectively. These intersections marked by black circles (A–T) refer to the specific deformation conditions during isothermal uniaxial compression).

dissipation region and the relatively high power dissipation region. As expected, there exist obvious differences about the contour distribution of power dissipation as well as the scope of instability region. This phenomenon becomes the most obvious in the case of deformation condition [marked by black circle (F)] with temperature of 698 K and strain rate of 0.01 s^{-1}. In the processing map based on the Prasad criterion, this deformation condition is within the instability region, while in the processing map based on the Murty criterion, it actually locates in the stability region.

3.4 Correlations of Processing Maps to Microstructure Characteristics

To further identify the appropriate processing window of as-homogenized Mg-8.5Gd-4.5Y-0.8Zn-0.4Zr alloy, microstructures of all deformed samples are analyzed and displayed in Fig. 7. It is obvious that under the low temperature of 673 K (Fig. 7a, b, c, and d), these pre-existing 14H LPSO phases in the shape of block are mostly survived after hot deformation. Moreover, many thin-platelet phases occur within deformed grains. A similar phenomenon during hot deformation of Mg-Gd-Y-Zn-Zr alloy has been reported by Zhang et al. (Ref 18). They claimed that these fine lamellar-shaped phases also belong to 14H LPSO phases, which are dynamically precipitated during hot deformation under appropriate deformation condition. In addition, due to the necessity of accommodating plastic strain within individual grains, some of these lamellar-shaped 14H LPSO phases undergo the kink deformation and form the kink bands. It is worth noting that the nucleation of fine DRX grains mainly occurs and locates around the boundaries of coarse un-DRX grains in Fig. 7(a), (b), (c), and (c). Meanwhile, the number of DRX grains decreases dramatically along with the increasing strain rate, resulting in the consumption of less deformation energy (Ref 25). This observation is responsible for the decreasing values of power dissipation in regions marked by black circles (A-C) of Fig. 6. Further microstructure observations on Fig. 7(b) and (d) demonstrate the occurrence of microcrack and/or flow localization within compressed samples, which serves as a remarkable sign of instability region during hot working of metallic materials (Ref 10). This issue

agrees well the predicted results about instability region in processing maps of Fig. 6.

The microstructure characteristics shown in Fig. 7(e), (f), (g), and (h) at temperature of 698 K are quite similar to the ones shown in Fig. 7(a), (b), (c), and (d). More attention is paid to the deformation condition (marked by black circle (F) in Fig. 6). Obviously, no microcrack and/or flow localization can be observed within compressed samples. This issue confirms that this deformation condition of 698 K/0.01 s^{-1} can be applied in the practical processing of as-homogenized Mg-8.5Gd-4.5Y-0.8Zn-0.4Zr alloy. Therefore, the constructed processing map based on the Prasad criterion is with less reliability by comparison with the one based on the Murty criterion at temperature of 698 K. Moreover, Fig. 7(i), (j), (k), and (l) at temperature of 723 K and Fig. 7(m), (n), (o), and (p) at temperature of 748 K collectively confirm that the increase of temperature benefits in accelerating the nucleation and growth process with respect to DRX grains, while the increase of strain rate does the opposite. This observation can explain the decreasing values of power dissipation in regions marked by black circles (I-L) and (M-P) of Fig. 6. Deformed microstructures of as-homogenized Mg-8.5Gd-4.5Y-0.8Zn-0.4Zr alloy at temperature of 773 K are shown in Fig. 7(q), (r), (s), and (t). Clearly, strain rates of 0.001, 0.01, and 0.1 s^{-1} contribute to the occurrence of complete DRX during isothermal uniaxial compression. Meanwhile, the coarsen of initial DRX grains occurs in Fig. 7(q) and (r). These issues finally result in lower values of power dissipation at strain rate of 0.001 and 0.01 s^{-1}, and larger value of power dissipation at strain rate of 0.1 s^{-1}, as depicted in Fig. 6. This phenomenon has also been reported in the work of Sun et al. (Ref 25). Moreover, the increasing strain rate cannot provide sufficient time for the occurrence of complete DRX, therefore the value of power dissipation at strain rate of 1 s^{-1} is smaller than the one at strain rate of 0.1 s^{-1}. This issue has been successfully predicted by the constructed processing map in Fig. 6.

Based on the aforementioned microstructure characterizations, it can be concluded that as for the Prasad criterion, the processing window is composed of region 1# (about 748-773 K, 0.01-0.1 s^{-1}) with peak power dissipation of 0.45 and region 2# (about 708-748 K, 0.001-0.01 s^{-1}) with peak power
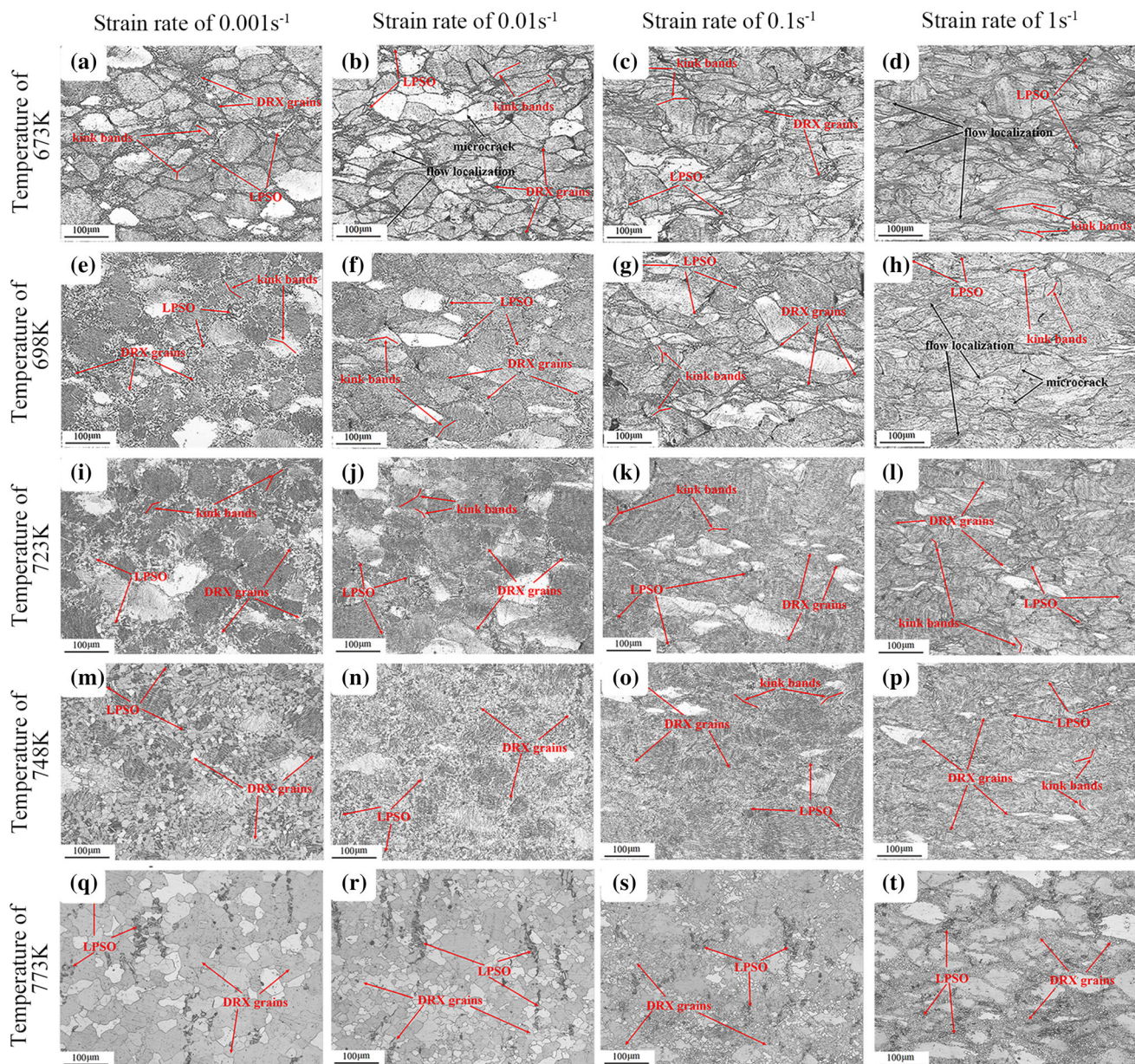
Fig. 7. Microstructures of as-homogenized Mg-8.5Gd-4.5Y-0.8Zn-0.4Zr alloy compressed to the true strain of 0.70: (a-d) At temperature of 673 K; (e-h) At temperature of 698 K; (i-l) At temperature of 723 K; (m-p) At temperature of 748 K; (q-t) At temperature of 773 K

dissipation of 0.45. With respect to the Murty criterion, the processing window is made up of region 3# (about 748-773 K, 0.01-0.1 s^{-1}) and region 4# (about 698-748 K, 0.01-0.1 s^{-1}). Both regions are with peak power dissipation of 0.47. Obviously, the processing windows based on these two criterions exist some differences, and the corresponding processing map based on the Murty criterion shows better consistency with experimentally observed microstructures and possesses broader processing parameters.

Although differences about processing windows based on the Prasad criterion and the Murty criterion are relatively small for the studied as-homogenized Mg-8.5Gd-4.5Y-0.8Zn-0.4Zr alloy, the present study still possesses valuable merits for the identification of optimized processing parameters for Mg-RE alloys with complex chemical compositions.

4. Conclusions

In the present study, the hot deformation behavior of as-homogenized Mg-8.5Gd-4.5Y-0.8Zn-0.4Zr alloy has been investigated via isothermal uniaxial compression tests at the temperature range of 673-773 K and the strain rate range of 0.001-1 s^{-1}. Based on the obtained true stress-strain curves, the processing maps based on the Prasad criterion and the Murty criterion are separately constructed and compared with each other. The following conclusions can be draw as follows:

The mechanical response of as-homogenized Mg-8.5Gd-4.5Y-0.8Zn-0.4Zr alloy during hot compression is the competing result of work hardening and work softening. The true stress-strain curve is sensitive to the deformation temperature and strain rate, namely it decreases with the decreasing strain

rate at a given temperature and increases with the decreasing temperature at a specific strain rate.

The distributions of power dissipation and the instability regime in the case of the Prasad criterion exist observable differences to the corresponding ones in the case of the Murty criterion with the proceeding of plastic deformation. Microstructure observation confirms that the instability region identified by the Murty criterion is more reliable than the one determined by the Prasad criterion.

For as-homogenized Mg-8.5Gd-4.5Y-0.8Zn-0.4Zr alloy, the processing map based on the Murty criterion is with more accuracy by comparison with the one based on the Prasad criterion. The correspondingly optimized processing window is identified to be 698-748 K, 0.001-0.01 s^{-1}, and 748-773 K, 0.01-0.1 s^{-1}.

References

1. J. Zhang, S. Liu, R. Wu, L. Hou and M. Zhang, Recent Developments in High-Strength Mg-RE-Based Alloys: Focusing on Mg-Gd and Mg-Y Systems, *J. Magnes. Alloys*, 2018, **6**(3), p 277–291.
2. H. Pan, Y. Ren, H. Fu, H. Zhao, L. Wang, X. Meng and G. Qin, Recent Developments in Rare-Earth Free Wrought Magnesium Alloys Having High Strength: A Review, *J. Alloys Compd.*, 2016, **663**, p 321–331.
3. X. Zhou, C. Liu, Y. Gao, S. Jiang, W. Liu and L. Lu, Hot Compression Behavior of the Mg-Gd-Y-Zn-Zr Alloy Filled with Intragranular Long-Period Stacking Ordered Phases, *J. Alloys Compd.*, 2017, **724**, p 528–536.
4. T. Homma, N. Kunito and S. Kamado, Fabrication of Extraordinary High-Strength Magnesium Alloy by Hot Extrusion, *Scr. Mater.*, 2009, **61**(6), p 644–647.
5. C. Xu, M. Zheng, S. Xu, K. Wu, E. Wang, S. Kamado, G. Wang and X. Lv, Ultra High-Strength Mg–Gd–Y–Zn–Zr Alloy Sheets Processed by Large-Strain Hot Rolling and Ageing, *Mater. Sc. Eng. A*, 2012, **547**, p 93–98.
6. M.H. Barezban, H. Mirzadeh, R. Roumina and R. Mahmudi, Constitutive Analysis of Wrought Mg-Gd Magnesium Alloys during Hot Compression at Elevated Temperatures, *J. Alloys Compd.*, 2019, **791**, p 1200–1206.
7. B. Zhang, L. Geng, L. Huang, X. Zhang and C. Dong, Enhanced Mechanical Properties in Fine-Grained Mg–1.0 Zn–0.5 Ca Alloys Prepared by Extrusion at Different Temperatures, *Scr. Mater.*, 2010, **63**(10), p 1024–1027.
8. Y. Sun, Z. Cao, Z. Wan, L. Hu, W. Ye, N. Li and C. Fan, 3D Processing Map and Hot Deformation Behavior of 6A02 Aluminum Alloy, *J. Alloys Compd.*, 2018, **742**, p 356–368.
9. J. Li, J. Liu and Z. Cui, Characterization of Hot Deformation Behavior of Extruded ZK60 Magnesium Alloy Using 3D Processing Maps, *Mater. Des.*, 2014, **56**, p 889–897.
10. Y. Xue, Z. Zhang, G. Lu, Z. Xie, Y. Yang and Y. Cui, Study on Flow Stress Model and Processing Map of Homogenized Mg-Gd-Y-Zn-Zr Alloy during Thermomechanical Processes, *J. Mater. Eng. Perform.*, 2015, **24**(2), p 964–971.
11. X. Shang, J. Zhou, X. Wang and Y. Luo, Optimizing and Identifying the Process Parameters of AZ31 Magnesium Alloy in Hot Compression on the Base of Processing Maps, *J. Alloys Compd.*, 2015, **629**, p 155–161.
12. C. Sun, G. Liu, Q. Zhang, R. Li and L. Wang, Determination of Hot Deformation Behavior and Processing Maps of IN 028 Alloy using Isothermal Hot Compression Test, *Mater. Sci. Eng. A*, 2014, **595**, p 92–98.
13. Y. Prasad, H. Gegel, S. Doraivelu, J. Malas, J. Morgan, K. Lark and D. Barker, Modeling of Dynamic Material Behavior in Hot Deformation: Forging of Ti-6242, *Metall. Trans. A*, 1984, **15**(10), p 1883–1892.
14. S.N. Murty and B.N. Rao, On the Flow Localization Concepts In the Processing Maps of Titanium Alloy Ti–24Al–20Nb, *J. Mater. Process. Technol.*, 2000, **104**(1–2), p 103–109.
15. Y. Prasad and T. Seshacharyulu, Processing Maps for Hot Working of Titanium Alloys, *Mater. Sc. Eng. A*, 1998, **243**(1–2), p 82–88.
16. S.N. Murty and B.N. Rao, On the Development of Instability Criteria during Hotworking with Reference to IN 718, *Mater. Sc. Eng. A*, 1998, **254**(1–2), p 76–82.
17. B. Li, B. Teng and W. Xu, Hot Deformation Characterization of Homogenized Mg-Gd-Y-Zn-Zr Alloy During Isothermal Compression, *JOM*, 2019, **71**(11), p 4059–4070.
18. Z. Zhang, Z. Yan, Y. Du, G. Zhang, J. Zhu, L. Ren and Y. Wang, Hot Deformation Behavior of Homogenized Mg-13.5 Gd-3.2 Y-2.3 Zn-0.5 Zr alloy via hot Compression Tests, *Materials*, 2018, **11**(11), p 2282.
19. Y. Wang, J. Peng, L. Zhong and F. Pan, Modeling and Application of Constitutive Model Considering the Compensation of Strain during Hot Deformation, *J. Alloys Compd.*, 2016, **681**, p 455–470.
20. C. Xu, J. Pan, T. Nakata, X. Qiao, Y. Chi, M. Zheng and S. Kamado, Hot compression deformation behavior of Mg-9Gd-2.9 Y-1.9 Zn-0.4 Zr-0.2 Ca (wt%) alloy, *Mater. Charact.*, 2017, **124**, p 40–49.
21. G. Zhou, Z. Li, D. Li, Y. Peng, H. Zurob and P. Wu, A Polycrystal Plasticity Based Discontinuous Dynamic Recrystallization Simulation Method and Its Application to Copper, *Int. J. Plast.*, 2017, **91**, p 48–76.
22. D.C. Hanselman and B. Littlefield, *The Student Edition of Matlab*, Prentice Hall, Hoboken, 1997
23. L. Xin, L. Shiqiang, W. Kelu, M. Fu, L. Zhenxi and C. Chunxiao, Hot Deformation Mechanism and Process Optimization for Ti-Alloy Ti-6.5 Al-3.5 Mo-1.5 Zr-0.3 Si during α+ β Forging Based on Murty Criterion, *Rare Met. Mater. Eng.*, 2008, **37**(4), p 577–583.
24. J. Shen, L. Hu, Y. Sun, X. Feng, A. Fang and Z. Wan, Hot Deformation Behaviors and Three-Dimensional Processing Map of a Nickel-Based Superalloy with Initial Dendrite Microstructure, *J. Alloys Compd.*, 2020, **822**, p 153735.
25. Y. Sun, X. Feng, L. Hu, H. Zhang and H. Zhang, Characterization on Hot Deformation Behavior of Ti-22Al-25Nb Alloy using a Combination of 3D Processing Maps and Finite Element Simulation Method, *J. Alloys Compd.*, 2018, **753**, p 256–271.